

Energy and exergy analysis of solar power tower plants

Chao Xu*, Zhifeng Wang, Xin Li, Feihu Sun

Key Laboratory of Solar Thermal Energy and Photovoltaic System, Institute of Electrical Engineering, Chinese Academy of Sciences, Beijing 100190, China

ARTICLE INFO

Article history:

Received 25 May 2011

Accepted 24 July 2011

Available online 29 July 2011

Keywords:

Exergy analysis

Solar power tower plant

Central receiver

Supercritical power cycle

ABSTRACT

Establishing the renewable electricity contribution from solar thermal power systems based on energy analysis alone cannot legitimately be complete unless the exergy concept becomes a part of that analysis. This paper presents a theoretical framework for the energy analysis and exergy analysis of the solar power tower system using molten salt as the heat transfer fluid. Both the energy losses and exergy losses in each component and in the overall system are evaluated to identify the causes and locations of the thermodynamic imperfection. Several design parameters including the direct normal irradiation (DNI), the concentration ratio, and the type of power cycle are also tested to evaluate their effects on the energy and exergy performance. The results show that the maximum exergy loss occurs in the receiver system, followed by the heliostat field system, although main energy loss occurs in the power cycle system. The energy and exergy efficiencies of the receiver and the overall system can be increased by increasing the DNI and the concentration ratio, but that increment in the efficiencies varies with the values of DNI and the concentration ratio. It is also found that the overall energy and exergy efficiencies of the solar tower system can be increased to some extent by integrating advanced power cycles including reheat Rankine cycles and supercritical Rankine cycles.

© 2011 Elsevier Ltd. All rights reserved.

1. Introduction

In the current world, electricity is still dominantly generated by burning conventional sources such as coal, oil and natural gas, which not only have a limited life but also release gaseous or liquid pollutants during operation. Because solar energy is an inexhaustible, clean and safe source of energy, it has received much attention as one of the most promising candidate to substitute for the conventional fuels for electricity supply [1–3]. Recently, rapid development occurred worldwide in the basic technology and market strategy for the concentrating solar power (CSP) technologies, including parabolic trough, power tower, and dish/engine. However, the power generation efficiencies of the CSP systems are found to be low, which indirectly increases the capital costs of electricity generation, and great efforts have to be concentrated on the future research and development of CSP systems.

In the power generation system, exergy analysis (or second law analysis) has proven to be a powerful tool in thermodynamic analyses of the system [4–11]. Exergy is defined as the maximum useful work that can be done by a system interacting with a reference environment. Different from the conventional energy analysis

that is based on the first law analysis, the exergy analysis can give a clearer assessment of various losses occurring in energy system both quantitatively and qualitatively. Exergy analysis can evaluate quantitatively the causes and locations of the thermodynamic imperfection in the energy system, and thus indicate the possibilities of thermodynamic improvement. As a result, exergy analysis has been widely used in the design, simulation and performance evaluation of energy systems. The conclusions from the exergy analysis play a significant role on improving the existing processes, components or systems, or developing new processes or systems.

Energy analysis (or first law analysis) method has been employed to conduct the energetic analysis and performance evaluation of the solar thermal power system or some components [1,2,12–19]. Yao et al. [1] carried out modeling and simulation of the pioneer 1 MW solar thermal central receiver system (CRS) in China (i.e., DAHAN). Based on the energy balance, they developed the mathematical models of the main basic components in the CRS and integrated them to be a whole plant model. Prakash et al. [16] carried out an experimental and numerical study of the steady state convective heat losses occurring from a downward facing cylindrical cavity receiver. Various fluid inlet temperatures and receiver inclinations were tested, and it was found that the convective loss increases with mean receiver temperature and decreases with the increase in receiver inclination. Montes et al. [17,18] investigated the influence of the solar multiple on the

* Corresponding author. Tel.: +86 10 82547036; fax: +86 10 62587946.
E-mail address: mechxu@gmail.com (C. Xu).

annual performance of parabolic trough solar thermal power plants with direct steam generation. Both thermal analysis and economic analysis were performed in their work. Larbi et al. [19] presented the performance analysis of a solar chimney power plant based on the energy balance, and they also investigated the effects of various factors on the thermal performance including the solar irradiance, the ambient temperature, the height of the tower, and the surface of the collector. Recently, Li et al. [2] developed a thermal model of molten salt cavity receiver based on the energy balance. Various factors, such as receiver area, heat loss, tube diameter, were analyzed to investigate the thermal performance of the cavity receiver.

However, very limited papers have appeared on the exergy analysis and performance assessment of the solar thermal power plant [4,5,10,20–22], which can offer insights not available from the energy analysis alone. Bejan et al. [4] analyzed the potential for exergy conservation in solar collector systems based on the second law of thermodynamics. It was shown that the exergy efficiency of the solar collector system is affected by heat transfer irreversibilities occurring between the sun and the collector, between the collector and the ambient air, and inside the collector. Kaushik et al. [5] presented an exergy analysis for a solar trough power plant. Basic energy and exergy analysis for the system components including parabolic trough collector/receiver and Rankine heat engine were carried out to evaluate the energy and exergy losses as well as exergy efficiency for typical solar thermal power system. It was found that the main exergy loss takes place at the collector-receiver assembly. You et al. [21] investigated the optimal thermal and exergy efficiencies for the combined system of the reheat-regenerative Rankine power cycle and the parabolic trough collector. It was found that, to make most advantage of the collector, the exiting fluid is supposed to be at the maximum temperature the collector can harvest. Lu et al. [10] established a basic physical model for solar absorber pipe with solar selective coating, based on which the associated heat transfer and exergy performances were analyzed and optimized. Most recently, Gupta et al. [22] carried out the energy and exergy analysis for the different components of a proposed conceptual direct steam generation solar tower power plant. It was found that the maximum energy loss takes place in the condenser followed by the solar collector field (including the trough concentrators and absorbers), while the maximum exergy loss occurs in the solar collector field.

The literature review indicates that the energy and exergy analysis of solar power tower plant, which uses heliostat field and central receiver as the concentrator-receiver system, has not been reported till now. In this regard, the objective of this article is to construct a theoretical framework for the energy and exergy analysis of the solar power tower plant using molten salt as the heat transfer fluid, which can be used to evaluate the energy and exergy losses in each component and in the overall power plant. The energy and exergy efficiencies have also been computed and compared for the individual components as well as for the overall plant. Several influencing factors including the direct normal irradiation (DNI), the concentration ratio, and the power cycle were also tested to evaluate their effects on the energy and exergy performance.

2. Energy and exergy analysis

Fig. 1 depicts the schematic of a solar power tower plant using molten salt as the heat transfer fluid. Since this paper only considers the energy and exergy performance of the system at steady state, the thermal storage subsystem will not be discussed and not shown in Fig. 1. Without considering the thermal storage

subsystem, the solar tower system can be considered as consisting of four subsystems: heliostat field subsystem, central receiver subsystem, steam generation subsystem (SGSS), and the conventional power cycle subsystem. The sun's rays fall on a field of mirrors known as heliostats, and are reflected into the aperture area of the central receiver, located at the top of a high tower, with the help of tracking system for each heliostat. The concentrated rays onto the central receiver result in high temperature of the receiver which is thus used to heat the molten salt flowing through the pipes embedded inside the receiver. Then the heated molten salt passes through the SGSS heat exchangers and transfers the thermal energy to the water which flows through the heat exchangers typically in a counter flow mode. After passing through the SGSS, water is heated from subcooled liquid to superheated steam, which is fed to the steam turbine for electricity generation.

The energy and exergy analysis of the whole system can be carried out by combining the analysis for each subsystem, which is in general based on the principle of energy and exergy balance for a control volume. The following assumptions are made in the analysis:

- The system runs at steady state with a constant solar isolation.
- Pressure drop and heat loss in pipe lines are all neglected.
- Kinetic and potential energy and exergy are ignored.
- Chemical exergy of materials are neglected.
- Parasitic efficiency of the whole system is assumed to be 88%, which is a typical value for systems of this kind.
- The efficiency of the power cycle is independent of the power output of the turbine.

For the steady-state process, the energy balance and exergy balance for a control volume can be expressed as Eqs. (1) and (2), respectively [23].

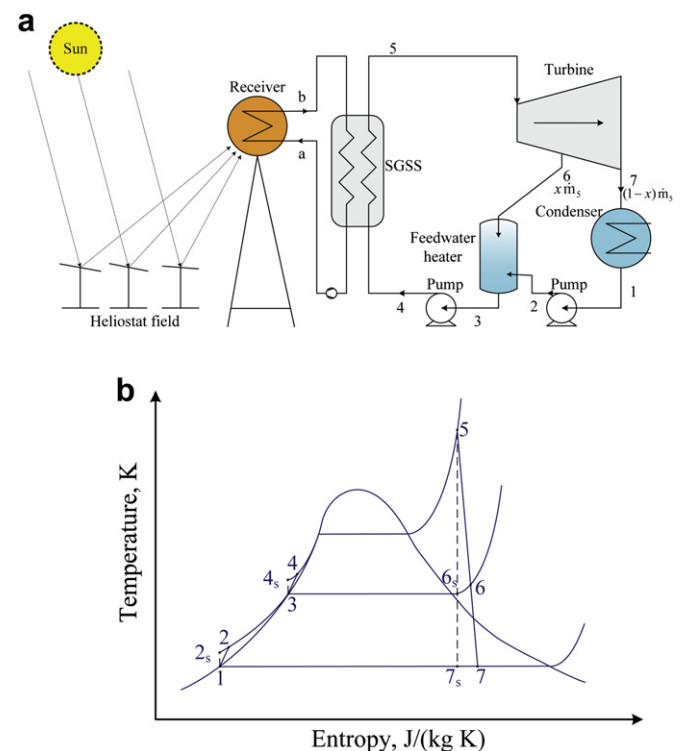


Fig. 1. Schematic of a solar tower power plant (a), and the temperature–entropy ($T-s$) diagram of the corresponding power cycle (power cycle 1).

$$\dot{W}_{c.v.} = \sum_j \dot{Q}_j + \sum_{in} \dot{m}_{in} h_{in} - \sum_{ex} \dot{m}_{ex} h_{ex} \quad (1)$$

$$\dot{W}_{c.v.} = \sum_j (1 - T_0/T_j) \dot{Q}_j + \sum_{in} \dot{m}_{in} \psi_{in} - \sum_{ex} \dot{m}_{ex} \psi_{ex} - T_0 \dot{S}_{gen} \quad (2)$$

where the exergy destruction ($T_0 \dot{S}_{gen}$), which is due to the entropy generation, is identical to the so-called irreversibility ($I\dot{R}$). The physical exergy of each state point can be considered as

$$\dot{\Psi} = \dot{m}\psi = \dot{m}((h - h_0) - T_0(s - s_0)) \quad (3)$$

Besides the above balance expressions, the energy efficiency and exergy efficiency, which refer to comparison of the desired output of a process with the input in terms of energy or exergy, are also used in the analysis. The analysis for each subsystem of the solar tower power plant is given as follows.

2.1. Heliostat field subsystem

The heliostat field, which consists of dozens or hundreds of heliostats and has a total aperture area of A_h , reflects and concentrates the sun's rays to the central receiver. The total isolation is proportional to the total area and can be given by $\dot{Q}^* = A_h \dot{q}^*$. Here \dot{q}^* means the amount of solar radiation received per unit area, which in this paper is treated as the direct normal irradiation (DNI). It should be noted that the DNI varies with several factors such as the geographical position on the earth, the meteorological condition, and the time of day. In the present analysis, it is assumed that \dot{q}^* is a constant and the system operates at steady state.

The incident solar radiation (\dot{Q}^*) is partly delivered to the central receiver as solar isolation \dot{Q}_{rec}^* by the heliostat field, while the remaining fraction (\dot{Q}_0^*) is lost to the environment due to various loss mechanisms. These mechanisms include losses due to cosine efficiency, blocking and shading, mirror reflectivity, tracking error, clean error, etc. [1]. In this analysis, it is assumed that the radiation energy loss is only accounted for by the overall field efficiency (η_h), which is defined as the ratio of the power incident on the receiver absorber surface to the power incident on the heliostats tracking the receiver. Thus, the energy balance and exergy balance for the heliostat field are given by

$$\dot{Q}^* = \dot{Q}_{rec}^* + \dot{Q}_0^* \quad (4)$$

$$\dot{\Psi}^* = \dot{\Psi}_{rec}^* + \dot{\Psi}_0^* \quad (5)$$

where $\dot{\Psi}_{rec}^*$ is the exergy delivered to the receiver and $\dot{\Psi}_0^*$ is the exergy loss (irreversibility).

The exergy $\dot{\Psi}^*$ associated with the solar irradiation on the heliostat mirror surface (\dot{Q}^*) can be expressed as

$$\dot{\Psi}^* = \dot{Q}^* (1 - T_0/T^*) \quad (6)$$

where T^* is the apparent sun temperature as an exergy source and taken to be 4500 K [4]. Similarly, the exergy delivered to the receiver is written as

$$\dot{\Psi}_{rec}^* = \dot{Q}_{rec}^* (1 - T_0/T^*) \quad (7)$$

Then, the energy efficiency and exergy efficiency of the heliostat field subsystem are given by Eqs. (8) and (9), respectively.

$$\eta_{l,h} = \dot{Q}_{rec}^*/\dot{Q}^* = \eta_h \quad (8)$$

$$\eta_{ll,h} = \dot{\Psi}_{rec}^*/\dot{\Psi}^* \quad (9)$$

2.2. Central receiver subsystem

The central receiver, which is typically installed at the top of the solar tower, has been developed with various shapes, including cavity receivers and cylindrical receivers. This analysis is only based on the cavity receiver. In operation, the receiver absorbs the isolation \dot{Q}_{rec} and transports part of the energy to the heat transfer fluid (e.g., molten salt) flowing through it. The rest of energy is lost to the environment by convective, emissive, reflective and conductive heat losses [2]. The energy balance and exergy balance for the central receiver are:

$$\dot{Q}_{rec}^* = \dot{Q}_{rec,abs} + \dot{Q}_{rec,totloss} = \dot{m}_{ms}(h_{ms,b} - h_{ms,a}) + \dot{Q}_{rec,totloss} \quad (10)$$

$$\dot{\Psi}_{rec}^* = \dot{\Psi}_{rec,abs} + \dot{\Psi}_{rec,loss} + I\dot{R}_{rec}^* \quad (11)$$

where the exergy loss associated with the heat loss is expressed as

$$\dot{\Psi}_{rec,loss} = \dot{Q}_{rec,totloss} (1 - T_0/T_{rec,sur}) \quad (12)$$

and the useful exergy absorbed by the flowing molten salt is

$$\begin{aligned} \dot{\Psi}_{rec,abs} &= \dot{m}_{ms}((h_b - h_a) - T_0(s_b - s_a)) \\ &= \dot{m}_{ms}c_{p,ms}(T_b - T_a - T_0 \ln(T_b/T_a)) \end{aligned} \quad (13)$$

The energy efficiency and exergy efficiency of the central receiver subsystem are defined as

$$\eta_{l,rec} = \dot{Q}_{rec,abs}/\dot{Q}_{rec}^* \quad (14)$$

$$\eta_{ll,rec} = \dot{\Psi}_{rec,abs}/\dot{\Psi}_{rec}^* \quad (15)$$

From the above analysis, in order to calculate the efficiency of the receiver, it is necessary to know the total heat loss from the receiver as well as the average surface temperature of the absorber. These can be determined by modifying a validated thermal model for designing molten salt cavity receivers developed by Li et al. [2]. Details about the modified model can be found in Appendix.

2.3. Steam generator subsystem (SGSS)

The SGSS usually consists of a series of heat exchangers, through which the high-temperature molten salt from the receiver heats water from the subcooled liquid to superheated steam. Assuming the heat exchangers are well insulated and the heat loss to the environment is negligible, the energy balance and exergy balance for the SGSS are

$$\dot{Q}_{rec,abs} = \dot{m}_{ms}(h_{ms,b} - h_{ms,a}) = \dot{Q}_{st,abs} = \dot{m}_{st}(h_{st,5} - h_{st,4}) \quad (16)$$

$$\dot{\Psi}_{rec,abs} = \dot{\Psi}_{st,abs} + I\dot{R}_{sgs} \quad (17)$$

where the useful exergy absorbed by the heated water is

$$\dot{\Psi}_{st,abs} = \dot{m}_{st}((h_5 - h_4) - T_0(s_5 - s_4)) \quad (18)$$

The energy efficiency and exergy efficiency of the SGSS are:

$$\eta_{l,sgs} = \dot{Q}_{st,abs}/\dot{Q}_{rec,abs} = 100\% \quad (19)$$

$$\eta_{ll,sgs} = \dot{\Psi}_{st,abs}/\dot{\Psi}_{rec,abs} \quad (20)$$

2.4. Power cycle subsystem

The power cycle used in the solar tower power plant is generally a conventional Rankine cycle, which is depicted in Fig. 1. The Rankine cycle mainly consists of high and low-pressure turbine stages, feed water heaters, condensers and pumps. A regenerative Rankine cycle, which uses feed water heaters, is employed here to avoid too low water temperature at the inlet of the SGSS (Point 4), which is necessary to prevent the solidification of molten salt in the SGSS. Only one stage of extraction is used in the present analysis for simplicity. Different power cycles will be discussed in the following sections and the power cycle shown in Fig. 1 is termed as System 1 hereafter. The corresponding temperature–entropy (T – s) diagram of System 1 is shown in Fig. 1b.

For the power cycle subsystem, the energy balance and exergy balance are

$$\dot{Q}_{st,abs} = \dot{W}_{net} + \dot{Q}_{ps,totloss} \quad (21)$$

$$\dot{\Psi}_{st,abs} = \dot{W}_{net} + \dot{\Psi}_{ps,totloss} \quad (22)$$

where the net output work (electricity) from the power cycle subsystem is

$$\dot{W}_{net} = \dot{W}_t - \dot{W}_{p1} - \dot{W}_{p2} \quad (23)$$

The energy efficiency and exergy efficiency of the power cycle are

$$\eta_{I,ps} = \dot{W}_{net} / \dot{Q}_{st,abs} \quad (24)$$

$$\eta_{II,ps} = \dot{W}_{net} / \dot{\Psi}_{st,abs} \quad (25)$$

Finally, the overall energy efficiency and exergy efficiency of the whole system can be defined as the ratio of net electricity output ($\dot{W}_{net}\eta_{para}$) from the whole system to the energy or exergy input associated with the solar irradiation on the heliostat surface, i.e.,

$$\eta_{I,overall} = \dot{W}_{net}\eta_{para} / \dot{Q}^* \quad (26)$$

$$\eta_{II,overall} = \dot{W}_{net}\eta_{para} / \dot{\Psi}^* \quad (27)$$

3. Results and discussion

3.1. Model validation

From the preceding section, it is known that the present analysis is based on the energy balance and exergy balance of each subsystem. The analysis for the SGSS heat exchangers and the Rankine power cycle depends only on the thermodynamic properties of molten salt and steam at each state as shown in Fig. 1, which is well developed and self-evident. The analysis for the central receiver is based on a thermal model, which is modified from a validated model developed by Li et al. [2]. To validate the modification, the present model was used to calculate the thermal performance of the Sandia National Laboratories' molten salt electric experiment (MSEE) based on the parameters provided in Ref. [2]. The calculated energy efficiency of the receiver is 87.77%, which agrees well with the predicted value of 87.73% from Li's work, and the experimental average efficiency of 87.5% from Bergan's experiments [24]. Therefore, the calculated results of the paper are reasonable, which are useful for guiding the design and operation of solar tower power plants.

3.2. Base case study

This section will give a general discussion about the energy and exergy analysis of the solar tower power plant based on System 1. The properties of the base case system and properties of System 1 are shown in Tables 1 and 2, respectively. The properties of molten salt (i.e., a mixture of 60 wt% NaNO₃ and 40 wt% KNO₃) are [25]:

$$\text{Density, } \rho \text{ (kg/m}^3\text{)} = 2090 - 0.636 \times T \text{ (}^\circ\text{C)} \quad (28)$$

$$\text{Specific heat } c_p \text{ (J/(kg K))} = 1443 + 0.172 \times T \text{ (}^\circ\text{C)} \quad (29)$$

$$\begin{aligned} \text{Thermal conductivity, } \lambda \text{ (W/(m K))} \\ = 0.443 + 1.9 \times 10^{-4} \times T \text{ (}^\circ\text{C)} \end{aligned} \quad (30)$$

The results of energy and exergy analysis of the base case system are listed in Table 3. The percentages of energy and exergy losses at each subsystem are shown in Fig. 2, which are the energy (exergy) losses at each subsystem divided by the total energy (exergy) losses of the whole system. From the energy analysis, it is found that the isolation energy of 8.0 MW can generate net output electricity of 1.83 MW from the base case solar tower power plant. The total energy efficiency of the whole system is 22.9%, while the subsystem energy efficiencies are 75%, 90%, 100% and 37.85% for the heliostat field, central receiver, SGSS and the power cycle, respectively. The power cycle subsystem has not only the lowest energy efficiency, but also the main energy loss. The percentage energy loss in the power cycle is as large as 53.8%, followed by 32.4% in the heliostat field and 9.7% in the central receiver.

However, the results of the exergy analysis show a distinct behavior. The total exergy efficiency of the whole system is 24.5%, while the subsystem exergy efficiencies are 75%, 55.5%, 89.8% and 74.5% for the heliostat field, central receiver, SGSS and the power cycle, respectively. The power cycle subsystem has a relatively large exergy efficiency (74.5%), and the corresponding percentage exergy loss is as small as 12.6%, although main energy loss occurs there. On the contrary, although the central receiver has a large energy efficiency and a small energy loss percentage (9.7%), it has the largest percentage exergy loss (44.2%), followed by 33.1% in the heliostat field subsystem. This is because the fact that solar isolation is the energy of very high quality ($T^* = 4500$ K from Eq. (6)), and great irreversibilities occur when the high-quality isolation is absorbed to be thermal energy with the temperature of about 700–900 K. As a result, the energy loss in the central receiver has high quality, i.e., containing a lot of exergy. On the contrary, although the power

Table 1
Properties of the base case solar tower power plant (System 1).

Subsystem	Properties	Values	Unit
Heliostat field	Beam radiation (DNI)	800	W m ⁻²
	Overall field efficiency	75%	–
	Total heliostat aperture area	10,000	m ²
Central receiver	Aperture area	12.5	m ²
	Inlet temperature of molten salt	290	°C
	Outlet temperature of molten salt	565	°C
	View factor	0.8	–
	Tube diameter	0.019	m
	Tube thickness	0.00165	m
	Emissivity	0.8	–
	Reflectivity	0.04	–
	Wind velocity	5.0	m s ⁻¹
SGSS	Inlet temperature of water	239	°C
	Outlet temperature of steam	552	°C
–	Ambient temperature	20	°C

Table 2
Properties of state points in different power cycles.

State point	System 1		System 2		System 3	
	Temperature (°C)	Pressure (kPa)	Temperature (°C)	Pressure (kPa)	Temperature (°C)	Pressure (kPa)
1	45.8	10	45.8	10	45.8	10
2s	45.9	3150	45.9	3150	45.9	3000
2	46.0	3150	46.0	3150	46.0	3000
3	236.6	3150	236.6	3150	233.8	3000
4s	238.7	12,600	238.7	12,600	238.4	24,000
4	239.0	12,600	239	12,600	239	24,000
5	552.0	12,600	552	12,600	552	24,000
6s	327.4	3150	327.4	3150	470.5	3000
6	353.5	3150	353.5	3150	481.6	3000
7s	45.8	10	45.8	10	45.8	10
7	45.8	10	45.8	10	45.8	10
8	–	–	327.1	2520	317.3	4800
9	–	–	552	2520	552	4800

cycle subsystem has the main energy loss, it has little exergy loss since the lost energy is of very low quality.

Hence, in the CSP system, great efforts should be concentrated to reduce the exergy loss in the central receiver subsystem, as well as the heliostat field subsystem. The factors affecting the exergy efficiency of the central receiver can be analyzed from the following expression for the exergy efficiency, which is developed based on Eqs. (7), (10), (13), and (15):

$$\eta_{II,rec} = \eta_{I,rec} \frac{1 - T_0 \ln(T_b/T_a)/(T_b - T_a)}{1 - T_0/T^*} \quad (31)$$

The above equation indicates that the exergy efficiency of the receiver depends on the energy efficiency of the receiver ($\eta_{I,rec}$), and the inlet (T_a) and outlet (T_b) temperatures of the molten salt. For the base case system, $\eta_{I,rec} = 90\%$, and from Table 1, the inlet and outlet molten salt temperatures are 290 and 565 °C, respectively. Hence, the exergy efficiency is $\eta_{II,rec} = 61.5\% \times \eta_{I,rec} = 55.4\%$. That means that even there is no energy loss from the receiver ($\eta_{I,rec} = 100\%$), the exergy efficiency cannot exceed 61.5% for the present temperature design of the molten salt. Since there is no great potential for the further improvement of the energy efficiency, the increase in the exergy efficiency depends mainly on the temperature design of the working fluid. Specifically, the outlet temperature of the working fluid should be greatly increased for further increasing the exergy efficiency of the receiver. For instance, when the outlet temperature is increased to 1000 °C, the exergy efficiency is $\eta_{II,rec} = 71\% \times \eta_{I,rec}$, meaning the ideal exergy efficiency is increased from 61.5 to 71% as a result of the increase in the outlet temperature from 565 to 1000 °C.

However, the increase in the outlet temperature of working fluid may be limited by material constraints of pipes and engine, which needs extensive future research work in this direction. Using the present working fluid, i.e., molten salt, the outlet temperature may be increased to some extent. Fig. 3 shows the variation in the energy and exergy efficiencies of the receiver when the outlet

temperature is increased from 565 to 645 °C. It is seen that, with the increase in the outlet temperature, the exergy efficiency can be slightly increased from 55.5 to 56.5%, while the energy efficiency is decreased from 90 to 88.5%. The decrease in the energy efficiency is due to the larger heat loss associated with higher receiver temperature. Therefore, when trying to increase the outlet temperature for improving the exergy efficiency, efforts must also be concentrated on lowering the energy loss, which becomes much trickier at higher working temperature.

3.3. Effect of incident solar isolation

The performance of the CSP plant depends highly on the incident solar isolation, which varies with the geographical position, the time of day, etc. To investigate the effect of incident solar isolation on the energy and exergy performance of the CSP system, different DNIs ranging from 100 to 1000 W m⁻² were tested in this work. Fig. 4 shows the variation in the energy and exergy efficiencies of both the receiver and the whole system as a function of the DNI. It is seen that both the energy and exergy efficiencies increase with the increase in the DNI. And the trend for the efficiency of the whole system is similar to that of the receiver, indicating that the effect of the DNI on the efficiencies of the whole system mainly depends on its effect on the efficiencies of the central receiver.

The increase in the energy and exergy efficiencies of the receiver with the DNI can be explained by analyzing the heat loss mechanism from the receiver. From Eqs. (A-2) and (A-4) in Appendix, two of the main heat loss mechanisms, i.e., emissive heat loss and convective heat loss, depend mainly on the surface temperature of the receiver, instead of the DNI. The change of surface temperature of the receiver with the DNI can be seen in Fig. 5, which shows clearly that when the DNI increases by ten times, from 100 to 1000 W m⁻², the surface temperature only varies slightly from 510 to 546 °C. As a result, the heat loss from the receiver only increases

Table 3
Energy and exergy analysis of the base case solar tower system.

Subsystem	Energy analysis				Exergy analysis			
	Received (kW)	Delivered (kW)	Loss (kW)	Energy efficiency (%)	Received (kW)	Delivered (kW)	Loss (kW)	Exergy efficiency (%)
Heliostat field	8000.0	6000.0	2000.0	75.00	7478.8	5609.1	1869.7	75.00
Central receiver	6000.0	5401.3	598.7	90.02	5609.1	3111.7	2497.4	55.48
SGSS	5401.3	5401.3	0.0	100.00	3111.7	2793.5	318.2	89.77
Power cycle	5401.3	2080.6	3320.7	37.85	2793.5	2080.6	712.9	74.48
Overall	8000	1830.9	6169.1	22.89	7478.8	1830.9	5647.9	24.48

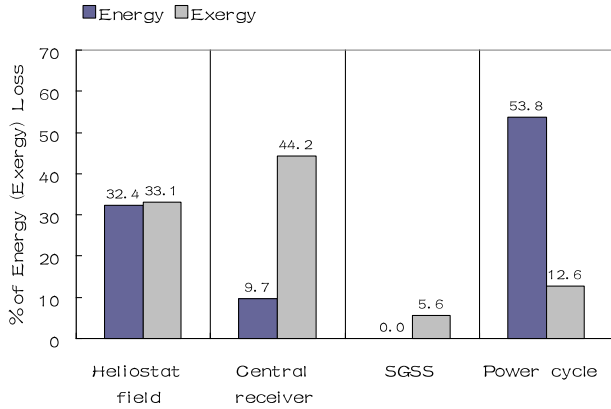


Fig. 2. Comparison of energy and exergy loss in the subsystems.

slightly when the input energy increases proportionally, which results in the increase in the energy and exergy efficiencies with the DNI. It should be pointed out that from Fig. 5 the surface temperature decreases first at very low solar isolation, e.g., $DNI < 200 \text{ W m}^{-2}$. This is due to the assumption that the molten salt is always heated from 290 to 565 °C through the receiver. When the DNI is very low, to maintain a fixed hot molten salt temperature at the receiver outlet, the molten salt flow rate should be very low, bringing less heat away and leaving more heat which heats up the receiver. Actually, this assumption becomes invalid when the DNI is decreased to a critical value, below which the molten salt cannot be heated to 565 °C even with a very low flow rate.

It is also seen that the effect of the DNI on the efficiencies varies with the values of DNI. For instance, the energy efficiency of the receiver increases greatly from about 45 to 85% when the DNI increases from 100 to 400 W m^{-2} , while it only increases slightly from 85 to 91% when the DNI increases further from 400 to 1000 W m^{-2} . The variation in the net output electricity with the DNI is also shown in Fig. 5. It is seen that the net output electricity increases nearly linearly from 100 to 2300 kW with the DNI increase from 100 to 1000 W m^{-2} .

3.4. Effect of concentration ratio

The concentration ratio of the receiver is a critical parameter when designing a high-efficient central receiver. To investigate the

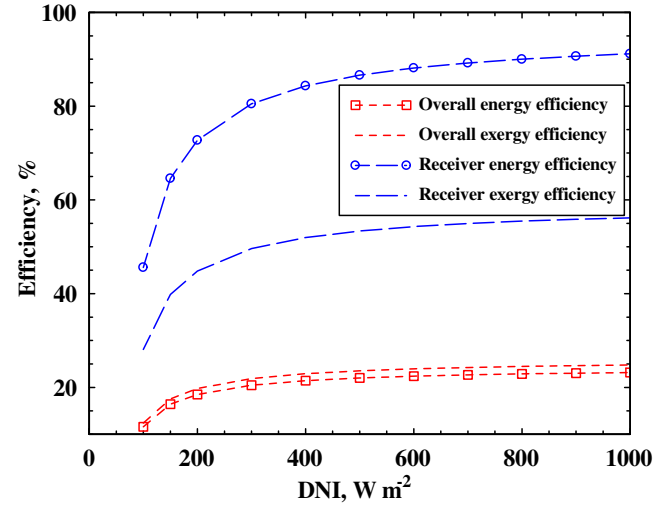


Fig. 4. Effect of the direct normal irradiation on the energy and exergy efficiencies of the receiver and the whole plant.

effect of concentration ratio on the energy and exergy performance, a large range of concentration ratios ranging from 200 to 1400 were tested. Fixing the total area of the heliostat field, with the increase in the concentration ratio, the open aperture area of the receiver decreases first sharply and then the decrease becomes slower, as shown in Fig. 6. Also, the concentration ratio affects the solar flux concentrated into the receiver, and thus the surface temperature of the receiver, which can be seen in Fig. 6. With the increase in the concentration ratio from 200 to 1400, the average surface temperature of the receiver increases nearly linearly from 456 to 618 °C, which can be easily understood by referring to Eq. (A-6).

The variation in the energy and exergy efficiencies of both the receiver and the whole system with the concentration ratio is shown in Fig. 7. Both the energy and exergy efficiencies increase with the increase in the concentration ratio. And similar to the effect of the DNI as discussed in the preceding section, the effect of the concentration ratio on the efficiencies of the whole system mainly depends on its effect on the efficiencies of the central receiver. With the increase in the concentration ratio, although the increased surface temperature of the receiver is disadvantageous for lowering the heat loss from the receiver, the simultaneous decrease in the aperture area plays a crucial role on lowering the

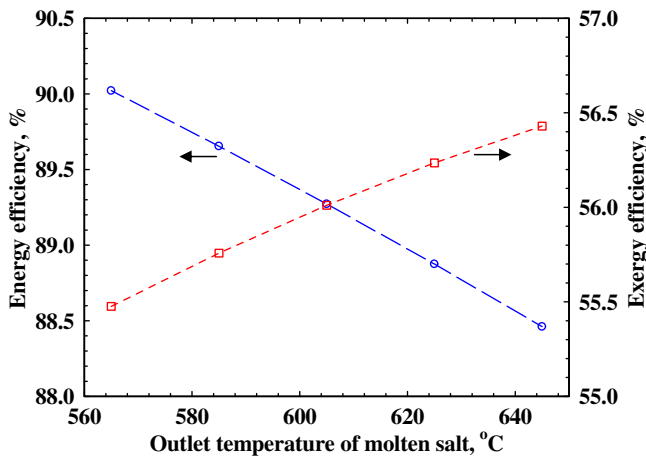


Fig. 3. Effect of the outlet temperature of the receiver on the energy and exergy efficiencies of the receiver.

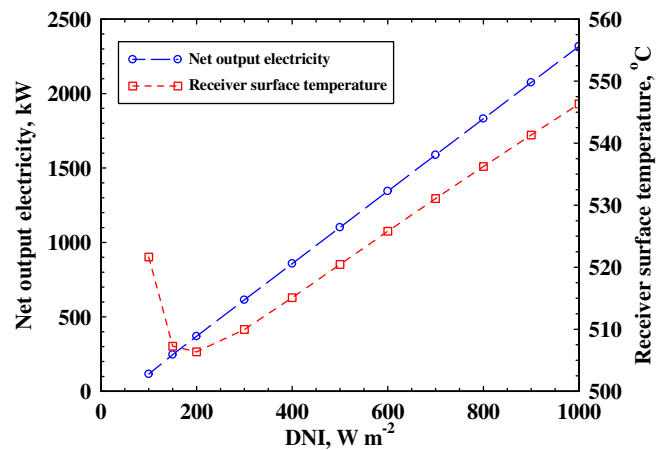


Fig. 5. Effect of the direct normal irradiation on the surface temperature of the receiver and net output electricity of the whole plant.

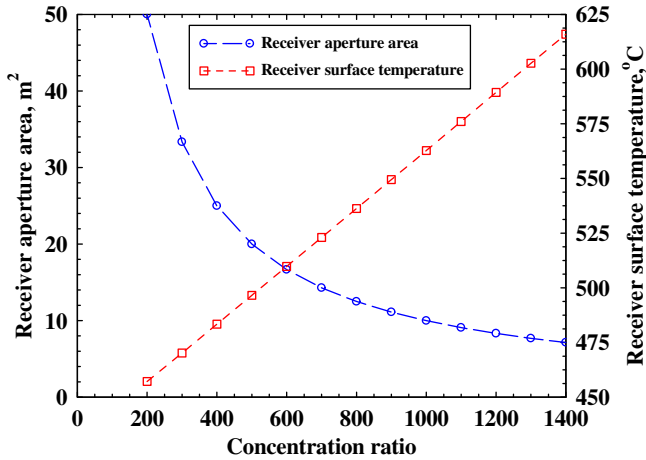


Fig. 6. Effect of the concentration on the aperture area and surface temperature of the receiver.

emissive, convective, and conductive heat loss as indicated by Eqs. (A-2), (A-4), and (A-5) in Appendix, which finally leads to a lowered total heat loss, and an increase in the energy efficiency and exergy efficiency.

It is also seen that the effect of the concentration ratio on the efficiencies varies with the values of concentration ratio. For instance, the exergy efficiency of the whole system increases evidently from 24.0% to 27.4% when the concentration ratio increases from 200 to 600, while it only increases slightly from 27.4% to 28.3% when the concentration ratio increases further from 600 to 1400. Therefore, the potential for further increasing the energy and exergy efficiencies becomes much less when the concentration ratio is beyond a critical value, e.g., 600 in this study.

3.5. Effect of advanced power cycle

As is known from the proceeding section, the receiver system accounts for most of the exergy loss, while the percentage exergy loss of the power cycle subsystem is much smaller, e.g., 12.6% for the base power cycle. However, great improvement in the exergy efficiency of the receiver system is impeded by the material

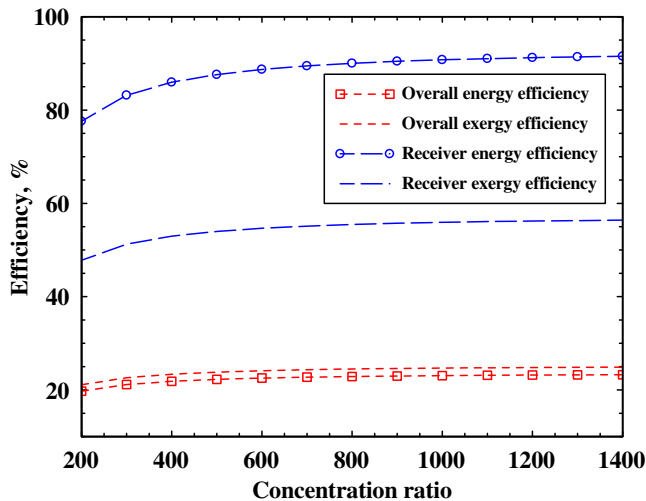


Fig. 7. Effect of the concentration ratio on the energy and exergy efficiencies of the receiver and the whole plant.

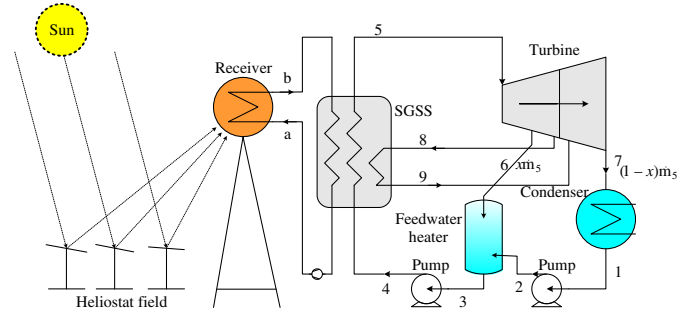


Fig. 8. Schematic of a solar tower power plant with a reheat process in the advanced power cycle (System 2 or 3).

constraints at high temperatures. Based on the state-of-the-art materials and technology, it is still effective to improve the energy and exergy efficiencies of the CSP system by improving the efficiency of the power cycle. In this section, we test two advanced power cycles: System 2 which has a reheat process, and System 3 which has a reheat process and has supercritical working steam. The schematic of the solar tower power plant with System 2 and System 3, and the corresponding $T-s$ diagrams are shown in Figs. 8 and 9, respectively. It should be noted that compared to System 1, System 2 has a reheat process: the steam is withdrawn from the exit of the high-pressure turbine and is reheated through the SGSS heat exchangers, after which the heated steam is fed to the low-

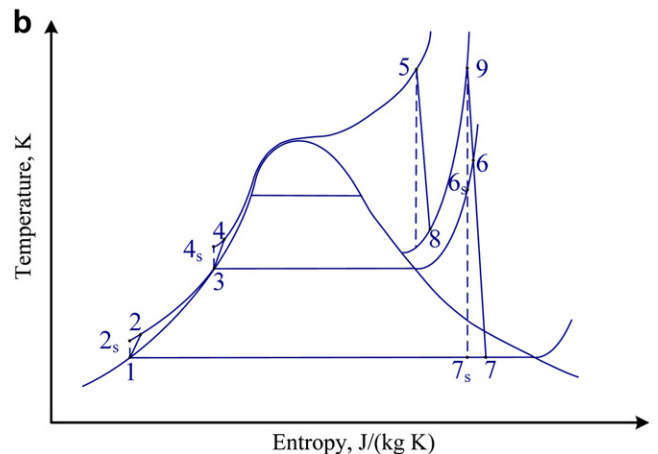
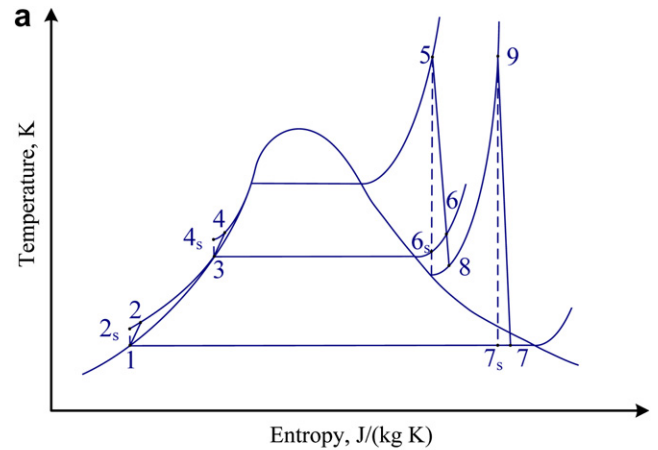


Fig. 9. Schematic of the temperature–entropy ($T-s$) diagrams of the advanced power cycles: System 2 (a) and System 3 (b).

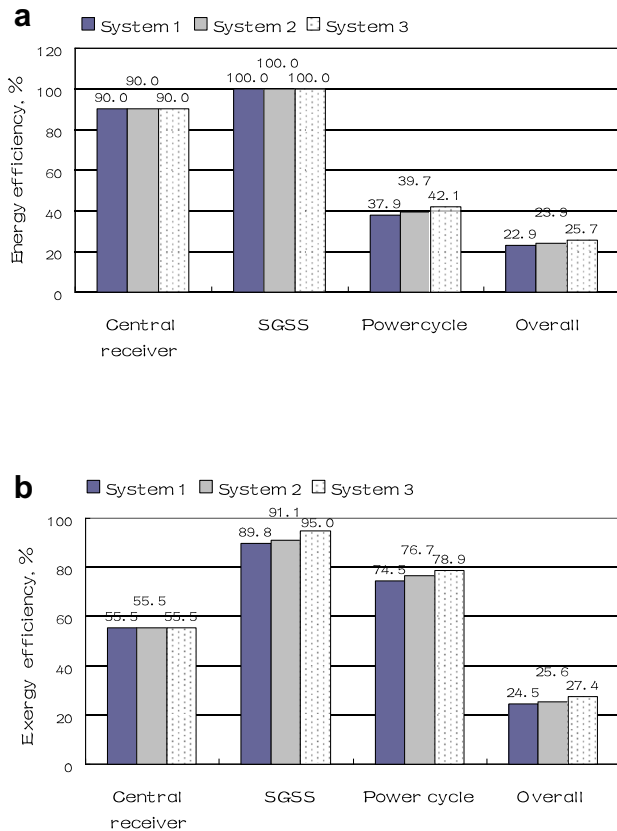


Fig. 10. Comparison of energy efficiency (a) and exergy efficiency (b) for the subsystems and the overall system using different power cycles.

pressure turbine. Compared to System 2, System 3 has a higher inlet steam pressure (i.e., 24 MPa) which makes the inlet steam to be supercritical steam. The reheat pressures in System 2 and System 3 are all chosen to be 20% of the inlet pressure of the high-pressure turbine.

Fig. 10 shows the energy and exergy efficiencies of individual components and the whole system using different power cycles (i.e., System 1, 2, and 3). For the energy efficiency, it is seen from Fig. 10a that the efficiency of power cycle increases from 37.9% to 39.7% after a reheat process is introduced (i.e., from System 1 to System 2). When the inlet steam becomes supercritical steam (in System 3), the energy efficiency of power cycle can be further improved to 42.1%. Accordingly, the overall efficiency of the solar tower plant increases evidently from 22.9% to 23.9% and then to 25.7% after System 1 is replaced by System 2 and System 3. While in terms of the exergy efficiency, it increases from 74.5% to 76.7% and to 78.9% for the power cycle when System 1 is updated to System 2 and System 3, respectively. Accordingly, the overall exergy efficiency of the solar tower plant increases from 24.5% to 25.6% after a reheat process is added, and further to 27.4% after the inlet steam becomes supercritical. Also, it should be pointed out that the tested power cycle with a reheat process (System 2) and the supercritical power cycle (System 3) are all not well optimized which are used here to illustrate the principle of the investigation of the advanced power cycles, and there is still some potential to further improve the efficiencies by optimizing the operating parameters. In general, the overall energy and exergy efficiencies can be increased to some extent by introducing the reheat process in the power cycle, and especially, using supercritical power cycle in the solar thermal tower plant.

On the other hand, it is also clear from Fig. 10b that the exergy efficiency of the SGSS can also be increased by using the advanced power cycle. For instance, it can be increased from 89.9% to 95.0% when System 1 is replaced by System 3. This is because that the average temperature difference for the heat transfer process is decreased in the advanced power cycle, which is obviously beneficial for improving the overall exergy efficiency of the solar tower plant.

4. Conclusions

In this paper, a theoretical framework for the energy and exergy analysis of the solar tower power plant using molten salt as the heat transfer fluid is developed. The energy and exergy losses in each component and in the overall power plant are evaluated to identify the causes and locations of the energy losses in the solar tower power plant. Salient findings and conclusions, which are valuable in the improvement of the solar tower power plant, are summarized as follows:

- 1) Due to the very low quality of energy losses from the power cycle subsystem, the power cycle subsystem has a relatively high exergy efficiency (74.5%), and the corresponding percentage exergy loss is as small as 12.6%, although main energy loss occurs there. On the other hand, although the central receiver has a high energy efficiency (90%) and a small energy loss percentage (9.7%), it has the largest percentage exergy loss (44.2%), followed by the heliostat field subsystem (33.1%). Therefore, in the solar power tower system, great efforts should be focused on reducing the exergy loss in the central receiver subsystem, which mainly depends on the operating temperature of the working fluid.
- 2) The effect of DNI on the energy and exergy efficiencies of the receiver, as well as the whole system, varies with the values of DNI. The energy efficiency increases greatly from about 45% to 85% when the DNI increases from 100 to 400 W m^{-2} , while it only increases slightly from 85% to 91% when the DNI increases further from 400 to 1000 W m^{-2} .
- 3) Fixing the total area of the heliostat field, with the increase in the concentration ratio, the decrease in the aperture area plays a crucial role on lowering the heat losses, which finally leads to an increase in the energy efficiency and exergy efficiency. Similarly, the effect of the concentration ratio on the efficiencies varies with the values of concentration ratio.
- 4) The overall energy and exergy efficiencies of the solar tower plant can be increased to some extent by introducing advanced power cycles. It is found that the overall exergy efficiency increases from 24.5% to 25.6% after a reheat process is added, and further to 27.4% after the inlet steam becomes supercritical.

Acknowledgements

This work has been financed by China's Ministry of Science and Technology under the National High Technology Development "863" Plan with Project No. (2006AA050101) and the National Basic Research Program of China (973 Program) with Project No. (2010CB227104), and Chinese Academy of Sciences.

Nomenclature

A	area, m^2
C	concentration ratio
c_p	specific heat, J (kg K)^{-1}
d	diameter, m

F_r	view factor
h	enthalpy, J kg^{-1} ; heat transfer coefficient, $\text{W (m}^2\text{K)}^{-1}$
$I\dot{R}$	irreversibility, W
\dot{m}	mass flow rate, kg s^{-1}
\dot{Q}	heat transferred, W
\dot{q}	heat flux, W m^{-2}
s	entropy, J kg^{-1}
T	temperature, K
W	work, W

Greek

δ	thickness, m
λ	thermal conductivity, W (m K)^{-1}
ε	receiver surface emissivity
σ	Stefan–Boltzmann constant $5.67 \times 10^{-8} \text{ W (m}^2\text{K}^4)^{-1}$
η	efficiency
ρ	density, kg m^{-3}
Ψ	exergy, W
ψ	exergy, J kg^{-1}

Superscripts

*	associated to solar rays
---	--------------------------

Subscripts

0	reference
abs	absorbed
avg	average
a	at the inlet
b	at the outlet
con	conduction
conv	convective
c.v.	control volume
em	emissive
ex	exit
fc	force convection
field	heliostat field
gen	generation
h	heliostat
I	the first law of thermodynamics
II	the second law of thermodynamics
in	inlet
i	inner
insi	inner side of receiver
ms	molten salt
nc	natural convection
o	outer
p	pump
para	parasitic
ps	power cycle
rec	receiver
ref	reflective
sgs	steam generation subsystem
st	steam
sur	surface
totloss	total loss
tube	tube for molten salt flow in the receiver

Appendix

A modified thermal model for the molten salt cavity receiver.

A simple introduction for the thermal model of designing molten salt cavity receivers is provided as follows, which is based on a validated thermal model developed by Li et al. [2].

The total heat losses from the central receiver can be contributed by different mechanisms, including convective, emissive, reflective, and conductive heat losses, which gives:

$$\dot{Q}_{\text{rec,totloss}} = \dot{Q}_{\text{rec,conv}} + \dot{Q}_{\text{rec,em}} + \dot{Q}_{\text{rec,ref}} + \dot{Q}_{\text{rec,con}} \quad (\text{A-1})$$

The expressions for the different heat losses are listed as follows:

$$\dot{Q}_{\text{rec,em}} = \varepsilon_{\text{avg}} \sigma (T_{\text{rec,sur}}^4 - T_0^4) A_{\text{field}} / C \quad (\text{A-2})$$

$$\dot{Q}_{\text{rec,ref}} = \dot{Q}_{\text{rec}}^* F_r \rho \quad (\text{A-3})$$

$$\dot{Q}_{\text{rec,conv}} = (h_{\text{air,fc,insi}}(T_{\text{rec,sur}} - T_0) + h_{\text{air,nc,insi}}(T_{\text{rec,sur}} - T_0) / F_r) A_{\text{field}} / C \quad (\text{A-4})$$

$$\dot{Q}_{\text{rec,con}} = \frac{(T_{\text{rec,sur}} - T_0) A_{\text{field}}}{(\delta_{\text{insu}} / \lambda_{\text{insu}} + 1 / h_{\text{air,o}}) F_r C} \quad (\text{A-5})$$

where the surface temperature of the absorber can be determined by the following equation:

$$\frac{\dot{Q}_{\text{rec}}^*}{A_{\text{field}} / F_r / C} = \frac{(T_{\text{rec,sur}} - T_{\text{ms}})}{d_o / d_i / h_{\text{ms}} + d_o \ln(d_o / d_i) / 2 / \lambda_{\text{tube}}} \quad (\text{A-6})$$

When the solar isolation reflected by the heliostat field to the receiver (\dot{Q}_{rec}^*) is known, the absorber's surface temperature, different heat losses, and the receiver thermal efficiency can be determined in an iteration manner shown by Li et al. [2]. For more information about the parameters and coefficients shown in Eqs. (A-1)–(A-6), please also refer to Li et al. [2] for the simplicity of this paper.

References

- [1] Z.H. Yao, Z.F. Wang, Z.W. Lu, X.D. Wei, Modeling and simulation of the pioneer 1 MW solar thermal central receiver system in China, *Renewable Energy* 34 (2009) 2437–2446.
- [2] X. Li, W.Q. Kong, Z.F. Wang, C. Chang, F.W. Bai, Thermal model and thermodynamic performance of molten salt cavity receiver, *Renewable Energy* 35 (2010) 981–988.
- [3] W. Han, H.G. Jin, J.F. Su, R.M. Lin, Z.F. Wang, Design of the first Chinese 1 MW solar-power tower demonstration plant, *International Journal of Green Energy* 6 (2009) 414–425.
- [4] A. Bejan, D.W. Kearney, F. Kreith, Second law analysis and synthesis of solar collector systems, *Journal of Solar Energy Engineering* 103 (1981) 23–28.
- [5] S.C. Kaushik, R.D. Misra, N. Singh, Second law analysis of a solar thermal power system, *International Journal of Solar Energy* 20 (2000) 239–253.
- [6] A. Hepbasli, A key review on exergetic analysis and assessment of renewable energy resources for a sustainable future, *Renewable and Sustainable Energy Reviews* 12 (2008) 593–661.
- [7] T. Ganapathy, N. Alagumurthi, R.P. Gakkhar, K. Murugesan, Exergy analysis of operating lignite fired thermal power plant, *Journal of Engineering Science and Technology Review* 2 (2009) 123–130.
- [8] Y.P. Dai, J.F. Wang, L. Gao, Exergy analysis, parametric analysis and optimization for a novel combined power and ejector refrigeration cycle, *Applied Thermal Engineering* 29 (2009) 1983–1990.
- [9] S. Farahat, F. Sarhaddi, H. Ajam, Exergetic optimization of flat plate solar collectors, *Renewable Energy* 34 (2009) 1169–1174.
- [10] J.F. Lu, J. Ding, J.P. Yang, Heat transfer performance and exergetic optimization for solar receiver pipe, *Renewable Energy* 35 (2010) 1477–1483.
- [11] R. Petela, Thermodynamic study of a simplified model of the solar chimney power plant, *Solar Energy* 83 (2009) 94–107.
- [12] J.E. Pacheco, M.E. Ralph, J.M. Chavez, Investigation of cold filling receiver panels and piping in molten-nitrate-salt central-receiver solar power plants, *Journal of Solar Energy Engineering* 117 (1995) 282–289.
- [13] S.A. Kalogirou, Solar thermal collectors and applications, *Progress in Energy and Combustion Science* 30 (2004) 231–295.
- [14] J.M. Lata, M. Rodríguez, M.Á. Lara, High flux central receivers of molten salts for the new generation of commercial stand-alone solar power plants, *Journal of Solar Energy Engineering* 130 (2008) 021002 (1–5).

- [15] T.Z. Ming, W. Liu, Y. Pan, G.L. Xu, Numerical analysis of flow and heat transfer characteristics in solar chimney power plants with energy storage layer, *Energy Conversion and Management* 49 (2008) 2872–2879.
- [16] M. Prakash, S.B. Kedare, J.K. Nayak, Investigations on heat losses from a solar cavity receiver, *Solar Energy* 83 (2009) 157–170.
- [17] M.J. Montes, A. Abánades, J.M. Martínez-Val, Performance of a direct steam generation solar thermal power plant for electricity production as a function of the solar multiple, *Solar Energy* 83 (2009) 679–689.
- [18] M.J. Montes, A. Abánades, J.M. Martínez-Val, M. Valdés, Solar multiple optimization for a solar-only thermal power plant, using oil as heat transfer fluid in the parabolic trough collectors, *Solar Energy* 83 (2009) 2165–2176.
- [19] S. Larbi, A. Bouhdjar, T. Chergui, Performance analysis of a solar chimney power plant in the southwestern region of Algeria, *Renewable and Sustainable Energy Reviews* 14 (2010) 470–477.
- [20] Y. Ying, E.J. Hu, Thermodynamic advantages of using solar energy in the regenerative Rankine power plant, *Applied Thermal Engineering* 19 (1999) 1173–1180.
- [21] Y. You, E.J. Hu, A medium-temperature solar thermal power system and its efficiency optimisation, *Applied Thermal Engineering* 22 (2002) 357–364.
- [22] M.K. Gupta, S.C. Kaushik, Exergy analysis and investigation for various feed water heaters of direct steam generation solar-thermal power plant, *Renewable Energy* 35 (2010) 1228–1235.
- [23] R.E. Sonntag, C. Borgnakke, G.J.V. Wylen, *Fundamentals of Thermodynamics*, sixth ed. John Wiley & Sons, Inc., 2003.
- [24] N.E. Bergan, An external molten salt solar central receiver test, *Solar Engineering* (1987).
- [25] A.B. Zavoico, *Solar Power Tower Design Basis Document*, Sandia National Laboratories, Report no. SAND2001–2100, 2001.